Chemical Engineering Journal 160 (2010) 33–41

Contents lists available at ScienceDirect

Chemical Engineering Journal

journal homepage: www.elsevier.com/locate/cej

Photocatalytic activity of La_2O_3-modified silver vanadates catalyst for Rhodamine B dye degradation under visible light irradiation

Hui Xu [a,b], Huaming Li [a,*], Guangsong Sun [a], Jiexiang Xia [b], Chundu Wu [b], Zhixiang Ye [c], Qi Zhang [a]

[a] School of Chemistry and Chemical Engineering, Jiangsu University, Zhenjiang 212013, PR China
[b] School of the Environment, Jiangsu University, Zhenjiang 212013, PR China
[c] College of Resource and Environment, Chengdu University of Information Technology, Chengdu 610225, PR China

ARTICLE INFO

Article history:
Received 1 August 2009
Received in revised form 10 February 2010
Accepted 25 February 2010

Keywords:
Photocatalytic
La_2O_3/Ag_3VO_4
Visible light irradiation
Degradation intermediates

ABSTRACT

La_2O_3/Ag_3VO_4 samples were synthesized by impregnation process and characterized by X-ray diffraction (XRD), scanning electron microscope (SEM), energy-dispersive X-ray spectroscopy (EDS), diffuse reflectance spectroscopy (DRS) and X-ray photoelectron spectroscopy (XPS). The XRD, SEM–EDS and XPS analyses revealed that La^{3+} was dispersed on Ag_3VO_4 in the form of La_2O_3 cluster. The DRS results indicated that the absorption edge of the La^{3+}–Ag_3VO_4 catalyst shifted to longer wavelength. The enhanced photocatalytic activity of La_2O_3/Ag_3VO_4 for Rhodamine B (RhB) dye degradation under visible light irradiation was due to its wider absorption edge and higher separation rate of photo-generated electron and holes. The highest photodegradation efficiency was obtained when the La_2O_3/Ag_3VO_4 catalyst was calcined at 300 °C with 3 wt% La content. The photocatalytic degradation intermediates of the solution were identified by LC/MS.

1. Introduction

Production of clean hydrogen energy and removal of environmental pollutants using photocatalysis technique have received a great deal of interest in recent few decades [1]. Photocatalytic reaction catalyzed by semiconductors has been approved as a promising process for solving energy and environmental issues [2]. Among the semiconductor catalysts, TiO_2 has been studied extensively owing to its special property [3]. However, the wide application of TiO_2 is limited in the condition of solar irradiation due to its wide band gap [4,5]. Therefore, considering energy conservation and environmental pollution issue, it is necessary and indispensable to develop high efficient and visible light-driven photocatalysts. Visible light-induced engineering includes modification of TiO_2 and development of new non-TiO_2-based environmental cleaning materials [6]. Recently, several new environmental cleaning materials including BiOBr [7,8], Bi_2WO_6 [9,10], and $BiVO_4$ [11–13] have been exploited.

Ag_3VO_4 with monoclinic structure has been fabricated and showed photocatalytic activity for water splitting and organic dyes degradation under visible light irradiation [14–16]. However, the photocatalytic activity of Ag_3VO_4 is still low due to its low separation rate of photo-generated electron and holes. Hu and Hu [15] present that the activity of the Ag_3VO_4 is increased by 11 times after doping NiO. It is indicated that the introduction of metal element can enhance the activity of the pure Ag_3VO_4. Recently, it is found that La could be used as cocatalyst, which proved to play a key role in increasing photocatalytic activity [17–20].

In the present work, La_2O_3/Ag_3VO_4 samples with different La concentrations and calcination temperatures are synthesized by impregnation technique. The photocatalytic activities of the samples are evaluated by Rhodamine B (RhB) dye degradation under visible light irradiation. The relationship between the photocatalytic activity and the structure property of the catalysts is discussed. The mechanism of enhanced photocatalytic activities after doping La^{3+} is also given. In addition, the photocatalytic degradation intermediates are identified by LC/MS, and the possible degradation process of RhB dye by La_2O_3/Ag_3VO_4 is proposed.

2. Experimental

2.1. Synthesis of the photocatalysts

Ag_3VO_4 was prepared by precipitation reaction as reported by Hu and Hu [15]. The La_2O_3/Ag_3VO_4 catalysts containing different La contents were prepared by impregnation method with the following procedure: firstly, a stoichiometric amount of La_2O_3 was dissolved in nitric acid (68%) solution. Secondly, 0.5 g of Ag_3VO_4 powder was added into the above $La(NO_3)_3$ solution. Then the suspension was stirred using a glass rod during evaporation of water

* Corresponding author. Tel.: +86 511 88791800; fax: +86 511 88791708.
E-mail address: lihm@ujs.edu.cn (H. Li).

1385-8947/$ – see front matter © 2010 Elsevier B.V. All rights reserved.
doi:10.1016/j.cej.2010.02.054

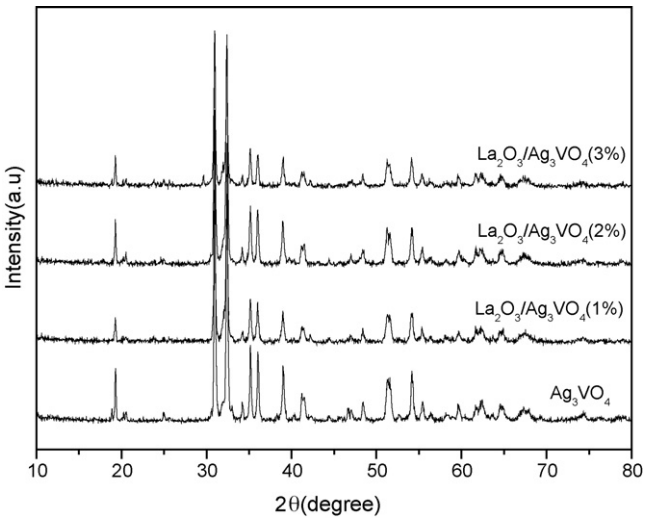

Fig. 1. XRD patterns of La_2O_3/Ag_3VO_4 samples with different La contents.

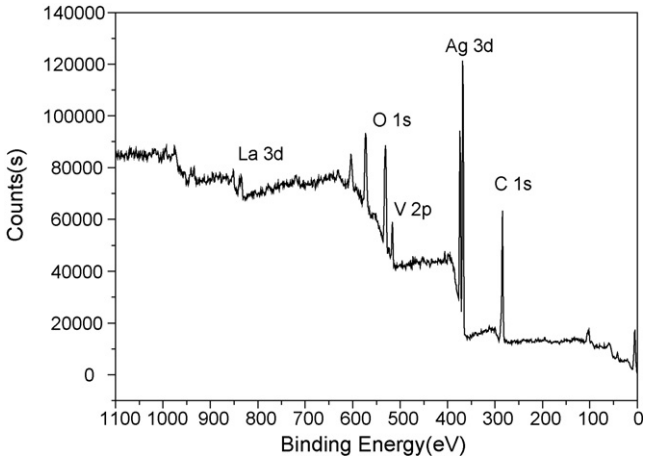

Fig. 3. XPS spectra of La_2O_3/Ag_3VO_4.

in a water bath. The as-synthesized La^{3+}–Ag_3VO_4 was calcined at 300 °C for 4 h. The pure Ag_3VO_4 catalyst was also calcined at 300 °C for 4 h.

2.2. Photocatalysts characterization

The crystalline phases of the prepared catalysts were analyzed by X-ray diffraction (XRD) by Bruker D8 diffractometer with CuKα radiation (λ = 1.54 Å) in the range of $2\theta = 10–80^\circ$.

The surface morphology and particle size of the samples were performed on a field emission scanning electron microscope (FESEM Model JEOL JSM-7001F). The elemental analysis of the photocatalysts was detected by an energy-dispersive X-ray spectrometer (EDS) attached to the SEM.

The X-ray photoelectron spectroscopy (XPS) measurement was performed on the ESCALab MKII spectrometer using MgKα radiation.

The diffuse reflectance spectra (DRS) were performed on a UV-2450 (Shimadzu) instrument in the range of 240–800 nm. $BaSO_4$ was used as the reflectance standard material.

2.3. Photocatalytic activity

The photocatalytic activities of La_2O_3/Ag_3VO_4 catalysts were evaluated by the degradation of RhB dye under visible light irradiation. The photocatalytic reactor consisted of a quartz glass with

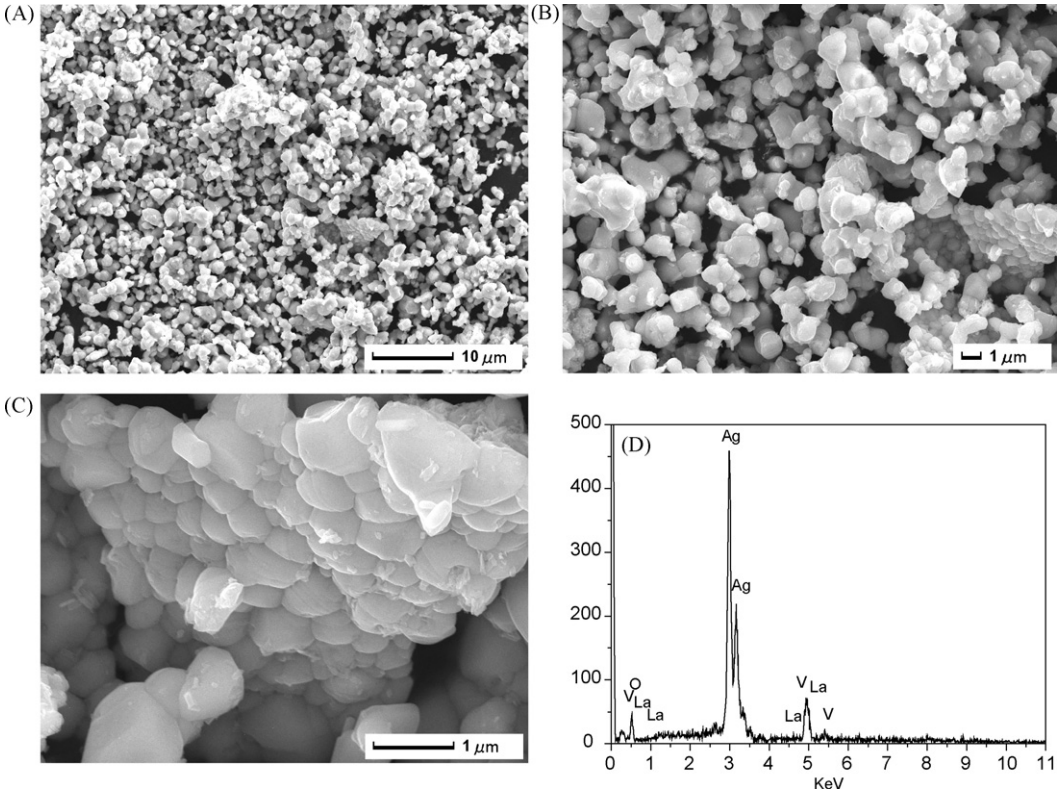

Fig. 2. Images of La_2O_3/Ag_3VO_4 sample (A–C), and (D) EDS spectrum of the La_2O_3/Ag_3VO_4.

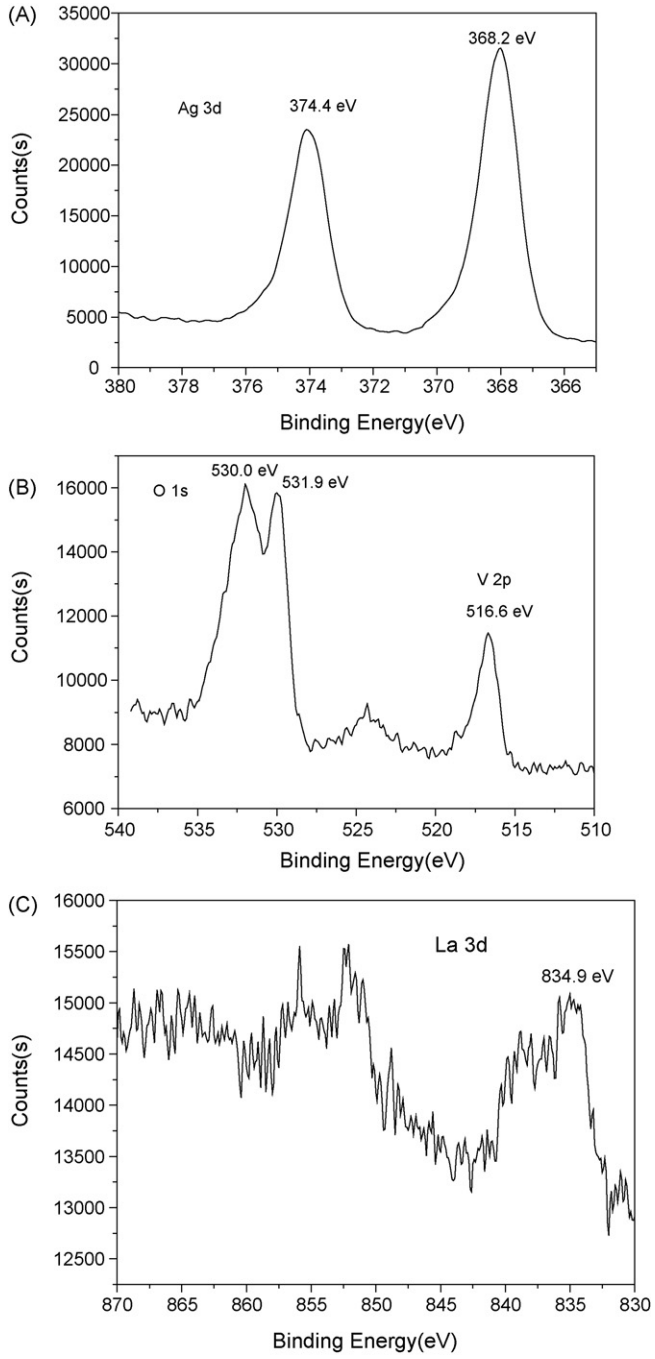

Fig. 4. High-resolution XPS spectra of (A) Ag 3d, (B) O 1s and V 2p, and (C) La 3d.

a circulating water jack and two 150-W tungsten halogen lamps as visible light source. In order to prevent the effect of thermal catalytic reaction, the temperature was kept at $25 \pm 1\,^{\circ}C$ by using inner air-compressor and the circulating water jack. 0.5 g/L of La_2O_3/Ag_3VO_4 was added to the RhB dye (initial concentration: 10 mg/L) solution. Prior to irradiation, the suspension was strongly magnetically stirred for 30 min in the dark for adsorption/desorption equilibrium. 5 mL suspension was taken at given time intervals and separated by centrifugation. The absorbance of RhB solution was determined by spectrophotometer at 553 nm. The photocatalytic degradation efficiency (E) of RhB was calculated by formula: $E = (A_0 - A)/A_0 \times 100\%$, where A_0 was the adsorption equilibrium absorbance of RhB and A was the absorbance of RhB solution at time t.

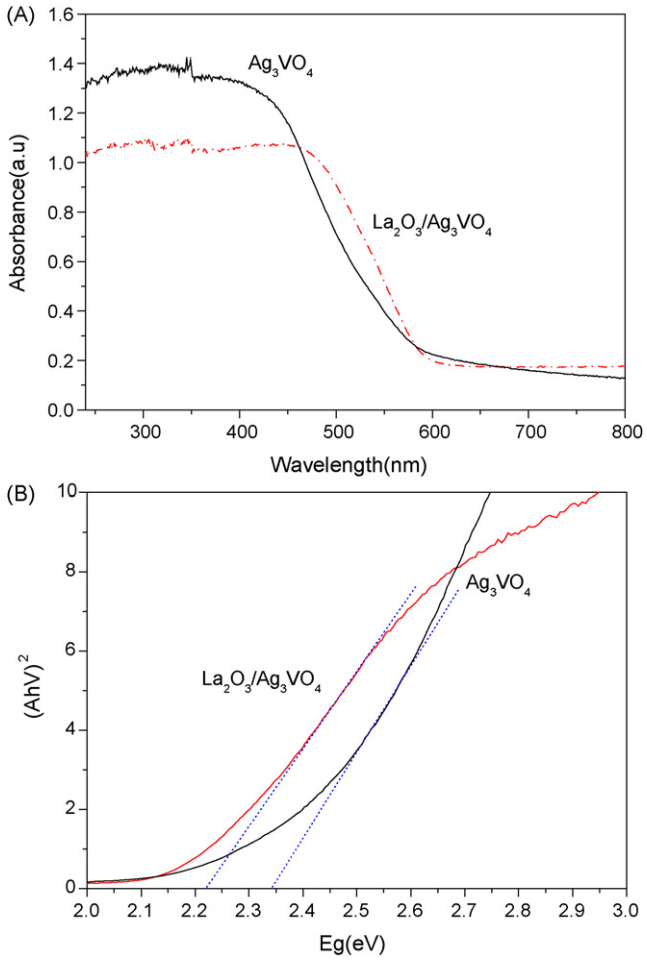

Fig. 5. DRS of Ag_3VO_4 and La_2O_3/Ag_3VO_4 photocatalysts (A) and estimated band gap of the samples (B).

2.4. Analytical methods

The *N*-de-ethylation intermediates of RhB were detected by high-performance liquid chromatography (HPLC) technique using a XDB-C18 column (5 μm, 4.6 mm × 150 mm) held at 30 °C. The HPLC separation was carried out using methanol as eluent sol-

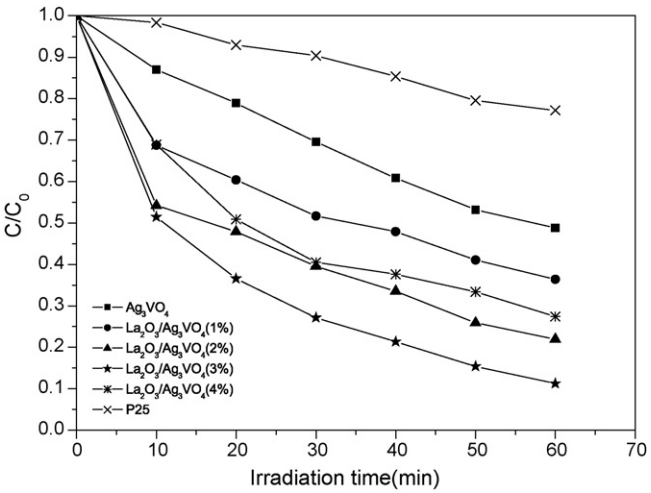

Fig. 6. Photocatalytic activities of La_2O_3/Ag_3VO_4 composites (0.5 g/L) with different La contents.

Table 1
Kinetic constants (k), the first order kinetic equation and relative coefficient (R) for the degradation of RhB under visible light irradiation.

Photocatalysts	Content of La^{3+} (wt%)	The first order kinetic equation	k ($\times 10^2$ min^{-1})	R
Pure Ag_3VO_4	0	$-\ln(C/C_0) = 0.00512 + 0.0122t$	1.22	0.999
La_2O_3/Ag_3VO_4	1	$-\ln(C/C_0) = 0.136 + 0.0154t$	1.54	0.974
La_2O_3/Ag_3VO_4	2	$-\ln(C/C_0) = 0.217 + 0.0214t$	2.14	0.968
La_2O_3/Ag_3VO_4	3	$-\ln(C/C_0) = 0.206 + 0.0340t$	3.40	0.988
La_2O_3/Ag_3VO_4	4	$-\ln(C/C_0) = 0.172 + 0.0198t$	1.98	0.970

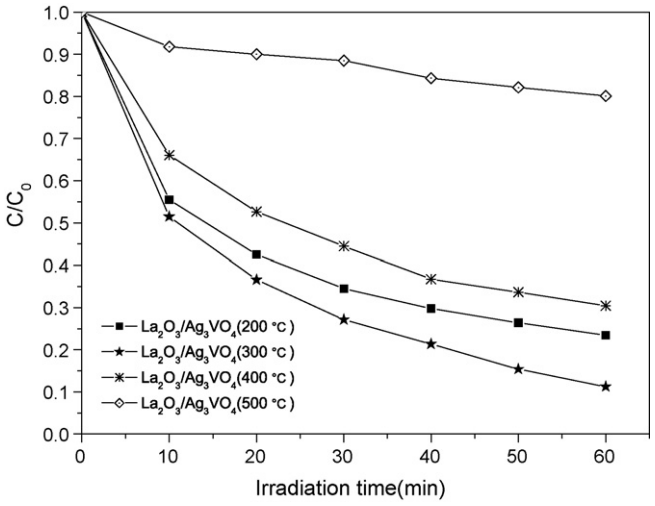

Fig. 7. Photocatalytic activities of La_2O_3/Ag_3VO_4 (3 wt%) composites calcined at different temperatures.

vent (from 60% to 90% methanol over 15 min) at a flow rate of 1 mL/min. Compounds were detected by a UV detector at the wavelength of 553 nm. LC/MS analysis was carried out using a commercial Thermo USA LCQ Deca XP max (Agilent Tc-c18 (4.6 mm × 150 mm)). The intermediates were also detected by an Agilent 6890N Gas Chromatograph with HP-5MS (Agilent 19091S-433: size 30 m × 0.25 μm) interfaced with an Agilent 5975 MSD analyzer.

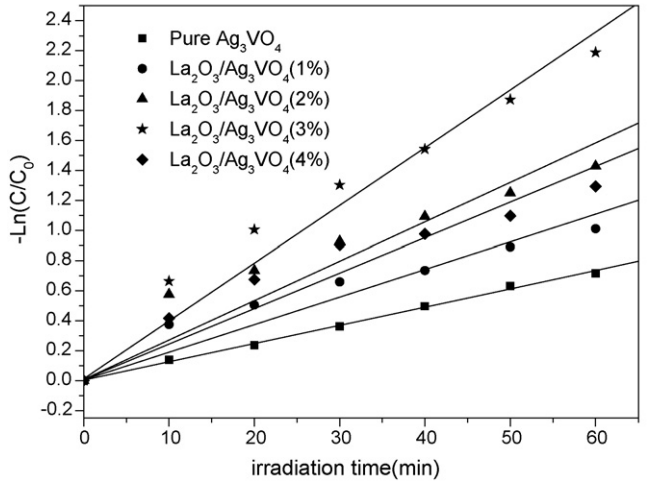

Fig. 8. Kinetic fit for the degradation of RhB with pure Ag_3VO_4 and La_2O_3/Ag_3VO_4 catalysts with different La^{3+} contents.

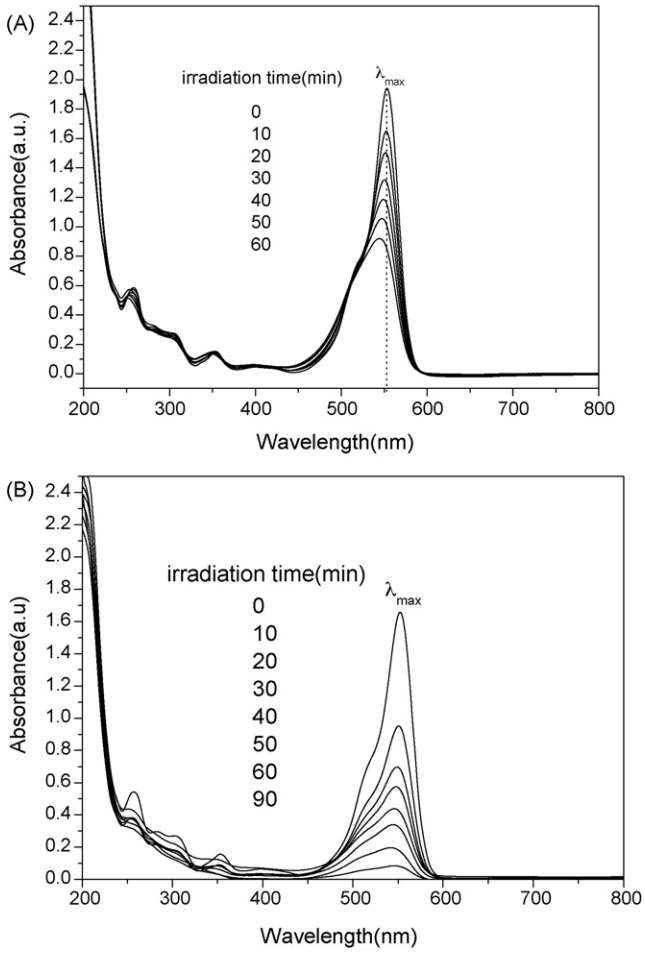

Fig. 9. Temporal UV–vis absorption spectral changes during the photocatalytic degradation of RhB in aqueous Ag_3VO_4 (A) and La_2O_3/Ag_3VO_4 (3 wt%) (B) under visible light irradiation.

3. Results and discussion

3.1. XRD analysis

The XRD patterns of La_2O_3/Ag_3VO_4 samples are shown in Fig. 1. It can be seen that all of the as-prepared samples appear to be Ag_3VO_4 monoclinic phase (JCPDS No. 43-0542). Further observation shows that the main diffraction peaks and their intensities of the catalysts do not give significant changes after doping La^{3+}, indicating the crystal structure of the samples keeps stable after doping La^{3+}. It is also found that there is no obvious difference between pure Ag_3VO_4 and La_2O_3/Ag_3VO_4 catalysts in terms of the lattice parameters '*a*' and '*c*', which indicates that La ions do not enter the lattice of Ag_3VO_4. However, the characteristic peaks of lanthanum oxides or La ion are not found in the XRD analysis attributed to the low lanthanum content.

3.2. SEM–EDS analysis

The morphology of La_2O_3/Ag_3VO_4 composite is shown in Fig. 2A–C. It is indicated that the sample is composed of many tiny particles, which is speculated to be the La_2O_3. The La^{3+} is probably present as La_2O_3 on the surface of the pure Ag_3VO_4, which will be discussed clearly in XPS analysis. The particles are agglomerated in irregular shape with particle size of ca. 0.5–1 μm. The EDS analysis shows that the sample is composed of Ag, V, O and La elements, as shown in Fig. 2D.

3.3. XPS

Although EDS characterization is effective in elemental analysis, it cannot discriminate the chemical states of elements. To identify the chemical state of La in the La^{3+}–Ag_3VO_4 composite, XPS is used to elucidate the La valence states. The full XPS spectra of La_2O_3/Ag_3VO_4 catalyst are shown in Fig. 3. It can be seen that the main peaks at 284.8, 531.9(530.0), 516.6, 368.2 and 834.9 eV are assigned to the binding energies of C 1s, O 1s, V 2p, Ag 3d and La 3d, respectively. Fig. 4 shows the high-resolution XPS spectra of the Ag 3d, O 1s, V 2p and La 3d regions. In Fig. 4A, it is found that there are two peaks at 374.4 and 368.2 eV, and these data are well corresponding to Ag 3d5/2 and Ag 3d3/2 binding energies, respectively, which is the characteristic of Ag^+ in Ag_3VO_4 [21]. V 2p orbit shows the splitting peak at 516.6 eV (Fig. 4B), which is corresponding to V 2p3/2 orbit. It is indicated that V exists as V^{5+} in the sample [6]. In Fig. 4B, it can be seen that the O 1s peak is fitted into two peaks centering at 531.9 and 530.0 eV, respectively. The peak at 530.0 eV is mainly assigned to the oxygen in the prepared sample lattice [22]. The peak centering at 531.9 eV corresponds to oxygen in the sample surface adsorption of (–OH) [23,24]. The XPS spectra in Fig. 4C confirm that the La species are present in the form of La_2O_3, corresponding to the binding energies of 834.9 in the La 3d5/2, which is consistent with the literature reported by Jia et al. [25]. It is worth to note that the binding energy of La 3d exhibits chemical shift to low binding energy direction, which is different to the value reported by Huo et al. [17] and Anandan et al. [26]. Compared with the standard XPS energy peak location of La 3d in La_2O_3, the obtained La 3d spectrum in La_2O_3/Ag_3VO_4 sample is also lower than the pure La_2O_3 [27], which can be ascribed to the interaction between Ag_3VO_4 and La_2O_3. In other words, it can be ascribed to the variation of the La^{3+} chemical surroundings. Therefore, in XPS analysis, it can be deduced that the La exists as La_2O_3 in La^{3+}–Ag_3VO_4 photocatalysts.

3.4. DRS analysis

The DRS spectra of pure Ag_3VO_4 and La_2O_3/Ag_3VO_4 (La content: 3 wt%) are shown in Fig. 5A. It is observed that the absorption edges of La_2O_3/Ag_3VO_4 shift to longer wavelength. This red shift phenomenon by metal ions doping is also present in other systems, such as $Pd/BiVO_4$ [28] and $Co_3O_4/BiVO_4$ [6]. Tayade et al. [29] also indicate that the absorption bands of all the impregnated TiO_2 (Fe, Co, Ni, Cu, Ag doping) catalysts have extended to longer wavelength. The observed red shift can be attributed to a charge-transfer transition between the metal ion and the TiO_2 conduction or valance band [29]. Xu et al. [30] and Fu et al. [31] also indicate that the red shift of the absorption band in visible light region after doping metal ions is beneficial to enhance the photocatalytic activity of the catalysts. The optical band gap of the prepared samples can be estimated by the following formula: $(Ah\nu)^2 = (h\nu - E_g)$ (for direct band gap material) [32,33]. By plotting $(Ah\nu)^2$ versus E_g, the band gap energies of Ag_3VO_4 and La_2O_3/Ag_3VO_4 are estimated to be 2.34 and 2.22 eV (Fig. 5B), respectively. So it can be inferred that the introduction of La_2O_3 might be beneficial to improve the photocatalytic performance of Ag_3VO_4 under visible light irradiation.

3.5. Photocatalytic activity

The influence of La content on photocatalytic activities of the catalysts is shown in Fig. 6. Photocatalytic degradation efficiency of RhB by pure Ag_3VO_4 and P25-TiO_2 is 51% and 23% in 60 min irradiation, respectively. After introduction of La^{3+}, the samples show enhanced photocatalytic activity. The photocatalytic activity of the catalysts strongly depends on surface properties, absorption properties, crystallinity and optical properties. In the case of La_2O_3/Ag_3VO_4, the enhanced photocatalytic activity can be explained in the following way: for one thing, the absorption wavelength range of La_2O_3/Ag_3VO_4 catalyst is shifted to longer wavelength, which can facilitate the absorption in the visible light region. Xu et al. [30] reports that a larger red shift might indicate that the catalyst absorbs more photons and the photocatalytic activity is enhanced. For the other thing, the beneficial effect of La^{3+} should be explained by considering the efficient separation of photoexcited electrons and holes [17,25,26]. It is reported that

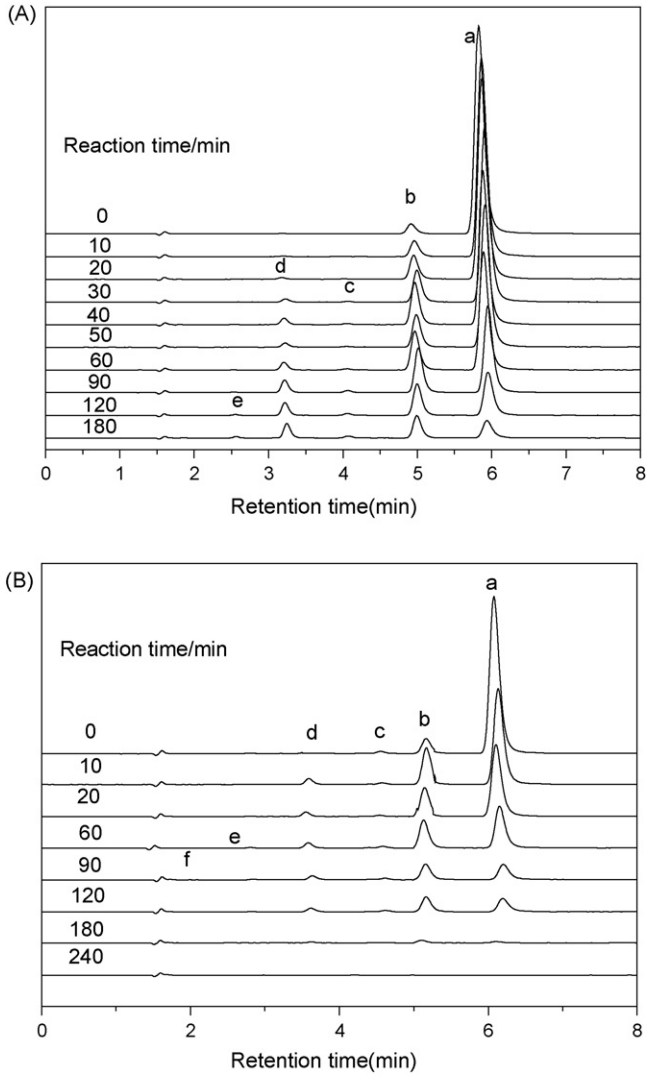

Fig. 10. HPLC chromatograms of the *N*-de-ethylated intermediates at different irradiation intervals: (A) in the role of pure Ag_3VO_4 (0.5 g/L); (B) in the role of La_2O_3/Ag_3VO_4 (La content: 3 wt%, 0.5 g/L).

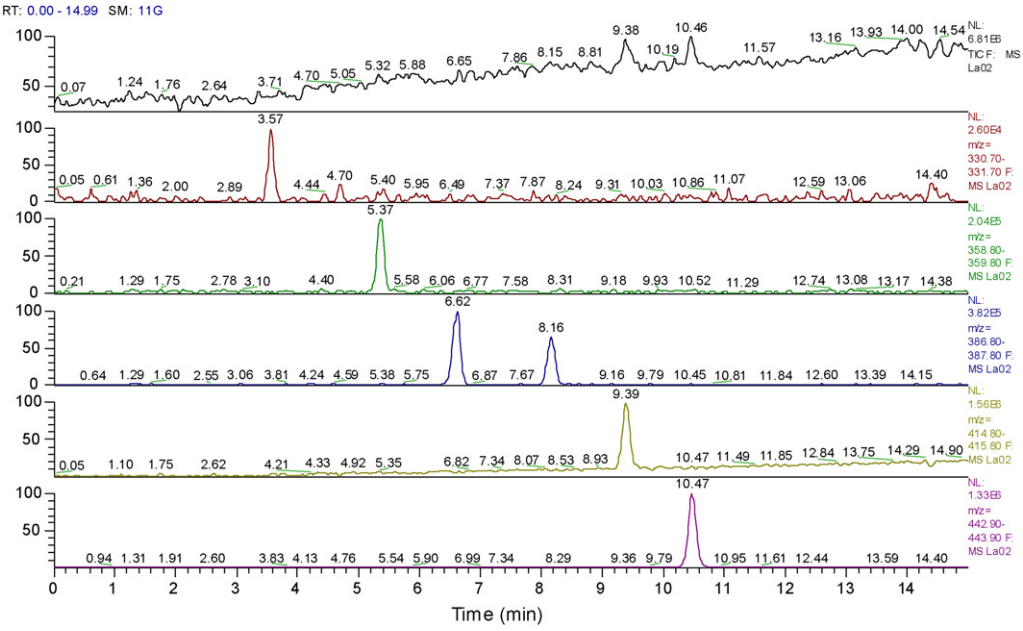

Fig. 11. LC/MS spectra of main products of the photocatalytic degradation of RhB.

La^{3+} can act as photo-generated electron trapper [17]. In the case of La_2O_3/Ag_3VO_4 catalyst, because of the ability of La_2O_3 trapping electrons, the La-modification can enhance the transfer and the separation rate of photo-generated electrons and holes. By the role of the La_2O_3, the generated electrons can quickly move from the Ag_3VO_4 to the surface. The enhanced separation rate of electron and hole can decrease the electron–hole recombination and improve the photocatalytic activity. The literatures also indicate that La^{3+} ion would be beneficial for the efficient separation of photo-generated electron–hole pairs [17,25,26]. Therefore, red shifts of the optical adsorption edge of Ag_3VO_4 by La_2O_3 doping and La_2O_3 used as electron trapper can enhance the visible light photocatalytic activity of the sample. Compared to the other system, the La_2O_3/Ag_3VO_4 has higher photocatalytic activity for RhB dye degradation, such as F-Bi_2WO_6 system [31]. After the irradiation for 60 min (300 W tungsten halogen lamps as light source), ca. 90% of RhB is degraded in the La_2O_3/Ag_3VO_4 system. However, in the F-Bi_2WO_6 system, 98% of RhB is degraded after 210 min visible light irradiation (500 W) [31].

It is interesting to note that the photocatalytic activities enhance with the increase in La content up to 3 wt% and then decrease. The optimum concentration of La^{3+} is required to match the thickness of charge layer and the depth of the light penetration. Similar result is also reported by Xu et al. [30]. In the case of La_2O_3/Ag_3VO_4 system, high La content (>3 wt%) is harmful for the photocatalytic activity due to the great coverage of active sites on the Ag_3VO_4 surface by La_2O_3 particles.

Fig. 7 shows the photocatalytic activities of La_2O_3/Ag_3VO_4 (3 wt%) composites calcined at different temperatures. The photoactivity of the samples follows the order: 300 °C > 200 °C > 400 °C > 500 °C. It is found that the calcination temperature play a vital role in the photocatalytic activity. In this work, the $La(NO_3)_3$ precursor is gradually decomposed into lanthanum oxide during calcinations process, and the degree of crystallization of La_2O_3 is enhanced by increasing the temperature. Generally, higher crystallinity of the sample is always beneficial for the separation of electron and hole pairs as compared to the amorphous structure [6]. As a consequence, the photocatalytic activity of the La_2O_3/Ag_3VO_4 is enhanced with increasing temperature. However, at higher calcination temperatures (≥400 °C), the La_2O_3 particle might be agglomerated, thus decrease photocatalytic activity of the sample. In addition, as the calcination temperature exceeds 400 °C, the crystallinity of the pure Ag_3VO_4 decreases (confirmed by XRD analysis). Therefore, the photocatalytic activity of the sample calcined at 500 °C is significantly decreased as compared to the catalyst prepared at 300 °C heat-treatment.

It is found that the photocatalytic degradation of RhB dye by La_2O_3/Ag_3VO_4 catalysts with different La^{3+} contents obeys pseudo-first-order kinetics. The linear plot of $-\ln(C/C_0)$ versus irradiation time t is shown in Fig. 8. The La^{3+}-doped samples show higher photocatalytic degradation rates than the pure Ag_3VO_4 catalyst. The photocatalytic degradation rate of La_2O_3/Ag_3VO_4 catalyst (3 wt%) is 2.8 times higher than that of the pure Ag_3VO_4. The pseudo-first-order constants, the first order kinetic equation and relative coefficients are summarized in Table 1.

3.6. Photodegradation of RhB and identification of the intermediates

The temporal evolution of the absorption spectral changes during the photocatalytic degradation of RhB by the pure Ag_3VO_4 and La_2O_3/Ag_3VO_4 are shown in Fig. 9. It is found that the absorption peak of the suspension decreases slowly in the case of Ag_3VO_4 catalyst (Fig. 9A). By contrast, in the presence of La_2O_3/Ag_3VO_4 catalyst (Fig. 9B), the absorption peak of RhB solution decreases significantly within 90 min irradiation. The color of the suspension changes colorless after 180 min. It is known that photocatalytic degradation of RhB dye occurs by two competitive pathways: *N*-de-ethylation and the cleavage of the conjugated structure [31,34,35]. To verify the photocatalytic degradation process, intermediate products during the photodegradation are detected by the HPLC technique, and the results are shown in Fig. 10. The five *N*-de-ethylated intermediates of the solution are identified by LC/MS, as shown in Fig. 11.

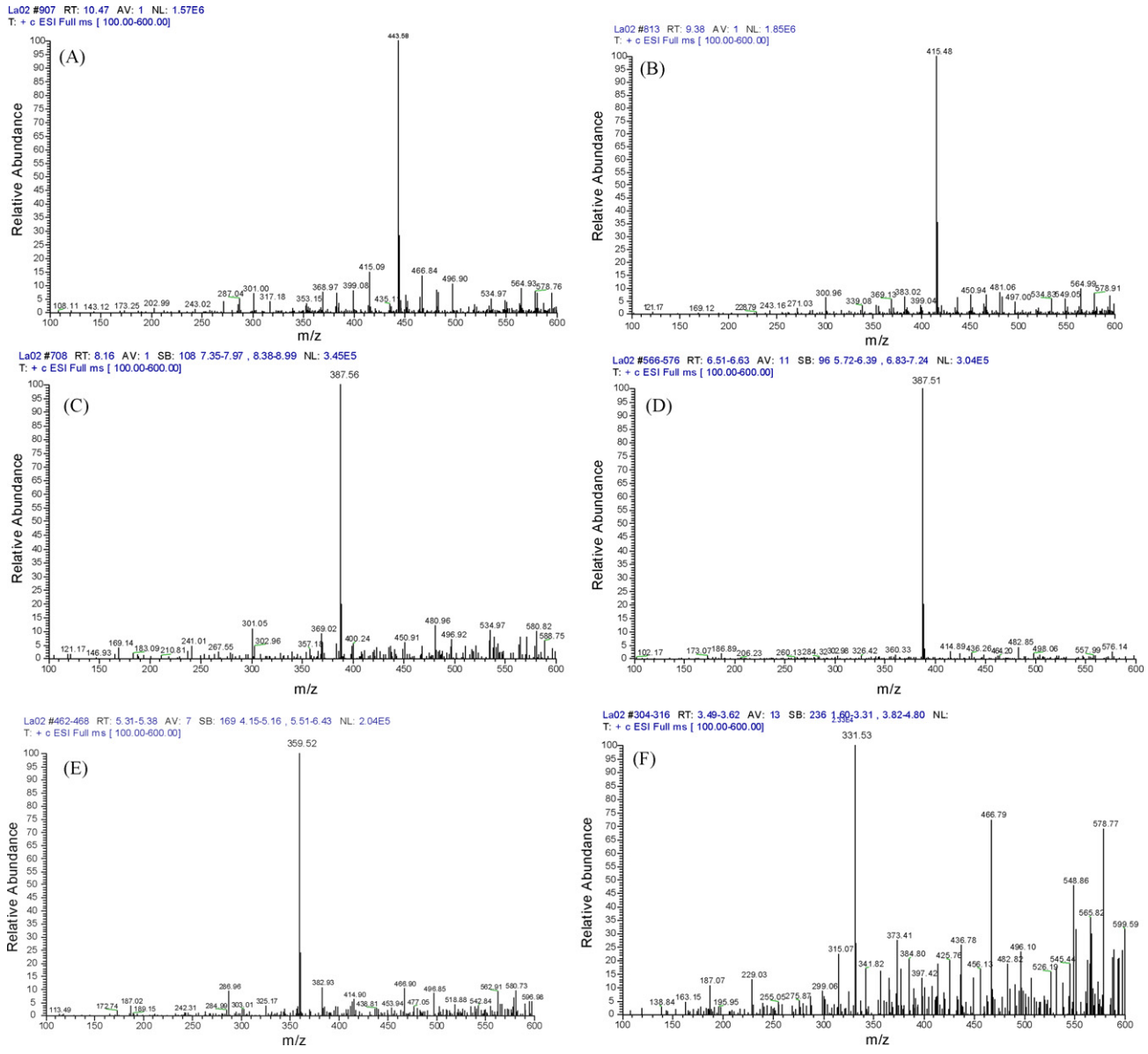

Fig. 12. Typical LC–MS chromatogram at the irradiation for 120 min (A: RhB; B: DER; C: EER; D: DR; E: ER; F: R).

Molecular-ion and fragment-ions of *N*-de-ethylated intermediates are shown in Fig. 12. Based on the polarity, retention time (in HPLC and LC/MS analyses, in Figs. 10 and 11) and mass spectra, peaks a–f have been identified as RhB, *N*,*N*-diethyl-*N*′-ethylrhodamine (DER), *N*,*N*-diethylrohodamine (DR), *N*-ethyl-*N*′-ethylrhodamine (EER), *N*-ethylrhodamine (ER) and Rhodamine (R), respectively. It is found that *m*/*z* of the major peak of "a" is at values of 443, corresponding to the RhB. Product b is identified with the major peak at the *m*/*z* value of 415, as shown in Figs. 11 and 12b. Products c and d are also detected at the *m*/*z* value of 387 (Figs. 11 and 12c and d), owing to the loss of the second ethyl groups on the RhB dye structures. Products e and f are found at the *m*/*z* value of 359 and 331, respectively (Figs. 11 and 12e and f), resulting from the further removal of the residual ethyl groups on the RhB dye structures. In the case of Ag_3VO_4 system, the b, c, d and e (*N*-de-ethylated intermediate, b, c, d and e are DER, EER, DR and ER, respectively) are detected. The concentration of the four intermediates is enhanced with irradiation time, and the peaks of b, c, d and e also present in the HPLC chromatograms after 180 min irradiation, indicating that the four intermediates cannot be degraded completely. In the presence of La_2O_3/Ag_3VO_4 catalyst, five intermediate products are observed, namely, DER, EER, DR, ER and R. The results indicate that the ethyl groups in the RhB structure are removed one by one, and finally transformed into R. The structure of RhB and the intermediates are listed in Table 2. In Fig. 10B, it is found that the concentrations of DER, EER, DR, ER and R species increase slightly and then all chromatogram peaks disappear after 180 min irradiation, which proved that RhB and the intermediates are degraded completely in La_2O_3/Ag_3VO_4/dye system. To provide more information about the small molecular weigh intermediates which cannot be identified by HPLC, the GC–MS technique is used to analyze the final products of RhB. However, the organic molecules including N-containing compounds are not detected in the solution. Therefore, it is deduced that the photodegradation of the RhB by La_2O_3/Ag_3VO_4 under the visible light irradiation is a stepwise *N*-de-ethylation process.

Table 2
Identification of RhB and *N*-de-ethylation intermediates by LC/MS.

Absorption peak	*m*/*z*	Retention time (min)	*N*-De-ethylation intermediates	Structural formula
a	443	10.47	Rhodamine B (RhB)	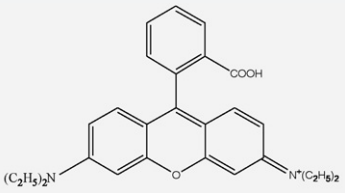
b	415	9.39	*N*,*N*-Diethyl-*N*′-thylrhodamine (DER)	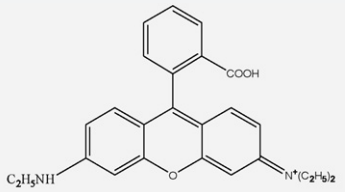
c	387	8.16	*N*-Ethyl-*N*′-ethylrhodamine (EER)	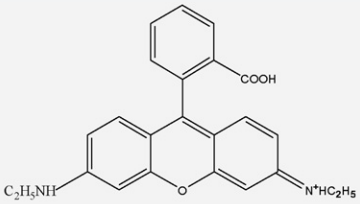
d	387	6.62	*N*,*N*-Diethylrohodamine (DR)	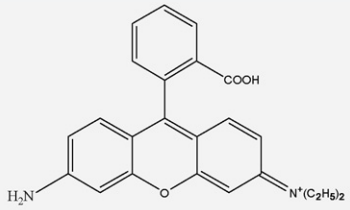
e	359	5.37	*N*-Ethylrhodamine (ER)	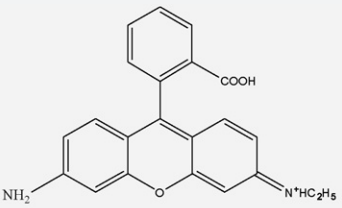
f	331	3.57	Rhodamine (R)	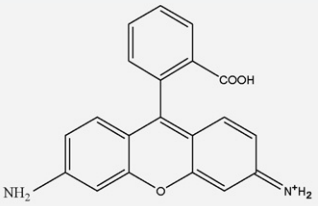

4. Conclusions

The prepared La_2O_3/Ag_3VO_4 catalysts showed higher photocatalytic efficiency for RhB degradation under visible light irradiation, and the optimal activity was obtained when the sample was calcined at 300 °C with 3 wt% La content. The enhanced photocatalytic activity of La_2O_3/Ag_3VO_4 was ascribed to its wider absorption edges and higher separation rate of electron and hole. LC/MS technique was used to analyze the degradation process, and photocatalytic degradation of RhB dye by La_2O_3/Ag_3VO_4 was mainly a stepwise *N*-de-ethylation process.

Acknowledgements

This work was supported by Doctoral Innovation Fund of Jiangsu (CX08B-142Z) and the National Nature Science Foundation of China (No. 20876071, 20676057 and 20871061).

References

[1] M. Anpo, M. Takeuchi, The design and development of highly reactive titanium oxide photocatalysts operating under visible light irradiation, J. Catal. 216 (2003) 505–516.
[2] X. Chen, S.S. Mao, Titanium dioxide nanomaterials: synthesis, properties, modifications, and applications, Chem. Rev. 107 (2007) 2891–2959.

[3] T.L. Thompson, J.T. Yates Jr., Surface science studies of the photoactivation of TiO_2—new photochemical processes, Chem. Rev. 106 (2006) 4428–4453.
[4] S.Y. Chai, Y.J. Kim, M.H. Jung, A.K. Chakraborty, D. Jung, W.I. Lee, Heterojunctioned $BiOCl/Bi_2O_3$, a new visible light photocatalyst, J. Catal. 262 (2009) 144–149.
[5] X. Li, J. Ye, Photocatalytic degradation of Rhodamine B over $Pb_3Nb_4O_{13}$/Fumed SiO_2 composite under visible light irradiation, J. Phys. Chem. C 111 (2007) 13109–13116.
[6] M. Long, W. Cai, J. Cai, B. Zhou, X. Chai, Y. Wu, Efficient photocatalytic degradation of phenol over $Co_3O_4/BiVO_4$ composite under visible light irradiation, J. Phys. Chem. B 110 (2006) 20211–20216.
[7] X. Zhang, Z. Ai, F. Jia, L. Zhang, Generalized one-pot synthesis, characterization, and photocatalytic activity of hierarchical BiOX (X = Cl, Br, I) nanoplate microspheres, J. Phys. Chem. C 112 (2008) 747–753.
[8] Z. Ai, W. Ho, S. Lee, L. Zhang, Efficient photocatalytic removal of NO in indoor air with hierarchical bismuth oxybromide nanoplate microspheres under visible light, Environ. Sci. Technol. 43 (2009) 4143–4150.
[9] Z. He, C. Sun, S. Yang, Y. Ding, H. He, Z. Wang, Photocatalytic degradation of rhodamine B by Bi_2WO_6 with electron accepting agent under microwave irradiation: mechanism and pathway, J. Hazard. Mater. 162 (2009) 1477–1486.
[10] F. Amano, K. Nogami, R. Abe, B. Ohtani, Preparation and characterization of bismuth tungstate polycrystalline flake-ball particles for photocatalytic reactions, J. Phys. Chem. C 112 (2008) 9320–9326.
[11] L. Zhang, D. Chen, X. Jiao, Monoclinic structured $BiVO_4$ nanosheets: hydrothermal preparation, formation mechanism, and coloristic and photocatalytic properties, J. Phys. Chem. B 110 (2006) 2668–2673.
[12] G. Li, D. Zhang, J. Yu, Ordered mesoporous $BiVO_4$ through nanocasting: a superior visible light-driven photocatalyst, Chem. Mater. 20 (2008) 3983–3992.
[13] S. Kohtani, M. Koshiko, A. Kudo, K. Tokumura, Y. Ishigaki, A. Toriba, K. Hayakawa, R. Nakagaki, Photodegradation of 4-alkylphenols using $BiVO_4$ photocatalyst under irradiation with visible light from a solar simulator, Appl. Catal. B: Environ. 46 (2003) 573–586.
[14] R. Konta, H. Kato, H. Kobayashi, A. Kudo, Photophysical properties and photocatalytic activities under visible light irradiation of silver vanadates, Phys. Chem. Chem. Phys. 5 (2003) 3061–3065.
[15] X. Hu, C. Hu, Preparation and visible-light photocatalytic activity of Ag_3VO_4 powders, J. Solid State Chem. 180 (2007) 725–732.
[16] X. Hu, C. Hu, J. Qu, Preparation and visible-light activity of silver vanadate for the degradation of pollutants, Mater. Res. Bull. 43 (2008) 2986–2997.
[17] Y. Huo, J. Zhu, J. Li, G. Li, H. Li, An active La/TiO_2 photocatalyst prepared by ultrasonication-assisted sol–gel method followed by treatment under supercritical conditions, J. Mol. Catal. A: Chem. 278 (2007) 237–243.
[18] G. Li, T. Kako, D. Wang, Z. Zou, J. Ye, Enhanced photocatalytic activity of La-doped $AgNbO_3$ under visible light irradiation, Dalton Trans. 13 (2009) 2423–2427.
[19] K. Dai, T. Peng, H. Chen, J. Liu, L. Zan, Photocatalytic degradation of commercial phoxim over La-doped TiO_2 nanoparticles in aqueous suspension, Environ. Sci. Technol. 43 (2009) 1540–1545.
[20] K.M. Parida, N. Sahu, Visible light induced photocatalytic activity of rare earth titania nanocomposites, J. Mol. Catal. A: Chem. 287 (2008) 151–158.
[21] J. Bai, Y. Li, M. Li, S. Wang, C. Zhang, Q. Yang, Electrospinning method for the preparation of silver chloride nanoparticles in PVP nanofiber, Appl. Surf. Sci. 254 (2008) 4520–4523.
[22] S. Chen, W. Zhao, W. Liu, H. Zhang, X. Yu, Y. Chen, Preparation, characterization and activity evaluation of p–n junction photocatalyst $p\text{-}CaFe_2O_4/n\text{-}Ag_3VO_4$ under visible light irradiation, J. Hazard. Mater. 172 (2009) 1415–1423.
[23] C.T. Campbell, Atomic and molecular oxygen adsorption on Ag(1 1 1), Surf. Sci. 157 (1985) 43–60.
[24] S.C. Hou, L.T. Liu, Y. Kou, $Li–ZnO/La_2O_3$ catalyst for the oxidation coupling of methane at low temperature, Acta Phys.: Chim. Sin. 22 (2006) 1040–1042.
[25] T. Jia, W. Wang, F. Long, Z. Fu, H. Wang, Q. Zhang, Fabrication, characterization and photocatalytic activity of La-doped ZnO nanowires, J. Alloys Compd. 484 (2009) 410–415.
[26] S. Anandan, A. Vinu, K.L.P. Sheeja Lovely, N. Gokulakrishnan, P. Srinivasu, T. Mori, V. Murugesan, V. Sivamurugan, K. Ariga, Photocatalytic activity of La-doped ZnO for the degradation of monocrotophos in aqueous suspension, J. Mol. Catal. A: Chem. 266 (2007) 149–157.
[27] E.R. Leite, A.P. Maciel, I.T. Weber, P.N. Lisboa-Filho, E. Longo, C.O. Paiva-Santos, A.V.C. Andrade, C.A. Pakoscimas, Y. Maniette, W.H. Schreiner, Development of metal oxide nanoparticles with high stability against particle growth using a metastable solid solution, Adv. Mater. 14 (2002) 905–908.
[28] L. Ge, Novel $Pd/BiVO_4$ composite photocatalysts for efficient degradation of methyl orange under visible light irradiation, Mater. Chem. Phys. 107 (2008) 465–470.
[29] R.J. Tayade, R.G. Kulkarni, R.V. Jasra, Transition metal ion impregnated mesoporous TiO_2 for photocatalytic degradation of organic contaminants in water, Ind. Eng. Chem. Res. 45 (2006) 5231–5238.
[30] A.W. Xu, Y. Gao, H.Q. Liu, The preparation, characterization, and their photocatalytic activities of rare-earth-doped TiO_2 nanoparticles, J. Catal. 207 (2002) 151–157.
[31] H. Fu, S. Zhang, T. Xu, Y. Zhu, J. Chen, Photocatalytic degradation of RhB by fluorinated Bi_2WO_6 and distributions of the intermediate products, Environ. Sci. Technol. 42 (2008) 2085–2091.
[32] H. Xu, H. Li, C. Wu, J. Chu, Y. Yan, H. Shu, Z. Gu, Preparation, characterization and photocatalytic properties of Cu-loaded $BiVO_4$, J. Hazard. Mater. 153 (2008) 877–884.
[33] H. Xu, H. Li, C. Wu, J. Chu, Y. Yan, H. Shu, Preparation, characterization and photocatalytic activity of transition metal-loaded $BiVO_4$, Mater. Sci. Eng. B 147 (2008) 52–56.
[34] P. Lei, C. Chen, J. Yang, W. Ma, J. Zhao, L. Zang, Degradation of dye pollutants by immobilized polyoxometalate with H_2O_2 under visible-light irradiation, Environ. Sci. Technol. 39 (2005) 8466–8474.
[35] C. Chen, W. Zhao, J. Li, J. Zhao, H. Hidaka, N. Serpone, Formation and identification of intermediates in the visible-light-assisted photodegradation of sulforhodamine-B dye in aqueous TiO_2 dispersion, Environ. Sci. Technol. 36 (2002) 3604–3611.